A new aluminum iron oxide Schottky photodiode designed via sol–gel coating method

A. Tataroğlu[a)†], A. A. Hendi[b)], R. H. Alorainy[b)], and F. Yakuphanoğlu[c)]

[a)]Department of Physics, Faculty of Science, Gazi University, Ankara, Turkey
[b)]Physics Department, Sciences Faculty for Girls, King Abdulaziz University, Jeddah, Saudi Arabia
[c)]Department of Physics, Faculty of Science, Fırat University, Elazığ, Turkey

(Received 11 July 2013; revised manuscript received 20 November 2013; published online 25 March 2014)

A novel aluminum iron oxide (Al/$AlFe_2O_4$/p-Si) Schottky photodiode was successfully fabricated via the sol–gel coating process. The microstructure of the spinel ferrite ($AlFe_2O_4$) was examined by atomic force microscopy. The current–voltage characteristics of the fabricated photodiode were studied under dark and different illumination conditions at room temperature. By using the thermionic emission theory, the forward bias I–V characteristics of the photodiode are analyzed to determine the main electrical parameters such as the ideality factor (n) and barrier height (Φ_{B0}) of the photodiode. The values of n and Φ_{B0} for all conditions are found to be about 7.00 and 0.76 eV, respectively. In addition, the values of series resistance (R_s) are determined using Cheung's method and Ohm's law. The values of R_s and shunt resistance (R_{sh}) are decreased with the increase of illumination intensity. These new spinel ferrites will open a new avenue to other spinel structure materials for optoelectronic devices in the near future.

Keywords: spinel ferrite, Schottky photodiode, I–V characteristics, barrier height

PACS: 75.50.Gg, 85.60.Dw, 84.37.+q, 73.30.+y **DOI:** 10.1088/1674-1056/23/5/057504

1. Introduction

Transparent conductive oxides (TCO) are doped metal oxides used in optoelectronic devices. Except for conventional semiconductors, transparent conducting oxides (TCO) are multifunctional oxide materials for Schottky diodes due to their wide optical band gap, and interesting electrical and optical properties.[1–4] These materials are very promising materials for opto-electrical devices such as sensors, phototransistors, diodes, solar cells, displays, opto-electrical interfaces, and circuitries.[5,6] TCO thin films were deposited using different techniques such as sol–gel, sputtering, and chemical vapor deposition.[7–12]

On the other hand, the spinel ferrites are important materials for electronics, communication applications and more.[12,13] Spinel ferrites have the general formula AFe_2O_4 (A = Mn, Co, Ni, Mg, Al, Zn) and they are very important magnetic materials due to their interesting magnetic and electrical properties.[13] These materials have been extensively used in various technological devices.[14] However, the performance of a Schottky diode depends on various factors such as the interface preparation process, the barrier height between the metal and the semiconductor, the surface preparation process, series resistance, temperature, illumination and applied bias voltage.[15–19]

It is well known that the semiconductor surface is usually covered with a thin layer of native oxide and organic contaminants in the laboratory environment or left in the box for enough time. Therefore, especially the series resistance (R_s), interface states or traps (N_{ss}) and a thin insulator layer play an important role on the performance of the Schottky barrier diode and similar electronic devices. The applied bias voltage and/or external electric field is also an important parameter which influences the main electrical parameters such as the ideality factor (n), the reverse saturation current (I_o), and barrier height (Φ_B). In general, the thermionic emission (TE) mechanism is used to extract the main diode parameters, and the forward-bias I–V characteristics may be given the information about the current-transport mechanism and barrier formation between metal and semiconductor. In addition, the forward-bias I–V characteristics usually deviate from the pure TE theory.[20–25] For example, the diode may exhibit a non-ideal behavior especially at a moderate bias region due to series resistance R_s, shunt resistance (R_{sh}), interfacial insulator or oxide layer and N_{ss}. The R_s is effective in the high bias region while the N_{ss} is effective in the low and moderate bias regions. Moreover, when the diode or photodiode is exposed to illumination intensity, electron-hole pairs occur near the junction and then they are separated under the electric field but this separation is more effective in the reverse bias region due to the high value of the electric field. Therefore, the photo-response effect in the reverse bias region is considerably higher than the forward bias region and the variation of photocurrent with light intensity was investigated in the reverse bias region at room temperature.

With the above lights, the goal of this study is to create novel metal/semiconductor junctions using spinel ferrites

†Corresponding author. E-mail: ademt@gazi.edu.tr

© 2014 Chinese Physical Society and IOP Publishing Ltd

($AlFe_2O_4$) for Schottky photodiodes applications. To our knowledge, there are not yet any experimental results on a Schottky diode of a spinel ferrites structure. Therefore, we successfully fabricated a new spinel ferrite (Al/$AlFe_2O_4$/p-Si) Schottky photodiode for the first time. Furthermore, the *I–V* characteristics of the Schottky photodiode under illumination conditions were examined in detail.

2. Experimental details

Al/$AlFe_2O_4$/p-Si Schottky photodiode was fabricated on p-type silicon (boron doped) crystal with ⟨111⟩ surface orientation, having a thickness of 600 μm and 5–10 Ω·cm resistivity, which correspond to 2.78×10^{15}–1.39×10^{15} cm^{-3} carrier concentration. Before the deposition process, a p-type crystalline silicon wafer was chemically etched by a solution of HF for 1 min and rinsed in re-distilled water using an ultrasonic bath for 10–15 min to remove the organic dirt. After that, it was rinsed in the ultrasonic bath by using high resistivity deionized water and was dried by pure nitrogen gas (N_2) to prevent surface oxidation. High purity (99.999%) aluminum (Al) was deposited on the whole back of the p-Si wafer in the high vacuum metal evaporation system at about 10^{-7} Torr (1 Torr ≈ 133.32237 Pa). In order to get a low resistivity ohmic contact, the wafer was annealed at about 570 °C for 5 min in N_2 atmosphere.

The aluminum nitrate ($Al(NO_3)_3$) and iron chloride ($FeCl_3$) were used as precursor materials and ethanol (CH_3CH_2OH) was used as the solvent. Firstly, the aluminum nitrate was dissolved in ethanol for 10 min and iron chloride and ethanol amine were added to this solution. The solution was stirred for 2 h at room temperature. The film was deposited onto the front side of the silicon wafer by spin coating with a rotating speed of 2000 rpm for 20 s. After each coating, the deposited sol was dried on a hot plate at 150 °C for 10 min to obtain a solid film. The coating procedure was repeated five times and dried. The obtained solid film was annealed at 400 °C for 2 h. After coating of $AlFe_2O_4$ film, the front of the rectifier/Schottky contacts were deposited on the Al/$AlFe_2O_4$/p-Si Schottky photodiode in the same vacuum metal evaporation system. The photodiode contact area was determined to be 3.14×10^{-2} cm^2.

The current–voltage (*I–V*) characteristics of the Al/$AlFe_2O_4$/p-Si Schottky photodiode were carried out using a Keithley 4200 semiconductor characterization system in the dark and in the illumination intensity range of 20–100 mW/cm^2 by 20 mW/cm^2 steps using a solar simulator. The intensity of the light was measured by a solar power meter (Model TM-206).

3. Results and discussion

The surface morphology of the $AlFe_2O_4$ film was examined with an atomic force microscope (AFM, Park System, and XE100) using the non-contact mode. A PARK system AFM XEI software programming was used to analyze the AFM images. As seen in Fig. 1, the $AlFe_2O_4$ film is formed from the particles like a pyramid. The thickness of the film is determined to be 35.01 nm.

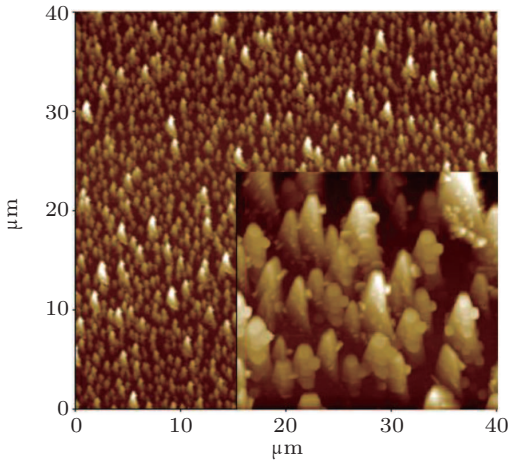


Fig. 1. (color online) AFM image of $AlFe_2O_4$ film.

The charge transport mechanism of the diode is analyzed using the thermionic emission (TE) theory. According to this theory, the current voltage characteristics of a Schottky diode can be analyzed by the following relation:[20,21]

$$I = I_0 \exp\left(\frac{q(V-IR_s)}{nkT}\right)\left[1-\exp\left(-\frac{q(V-IR_s)}{kT}\right)\right], \quad (1)$$

where V is the applied voltage, q is the electronic charge, k is the Boltzmann constant, T is the temperature, R_s is the series resistance, and I_0 is the reverse saturation current and it is defined as

$$I_0 = AA^*T^2\exp\left(-\frac{q\Phi_{B0}}{kT}\right), \quad (2)$$

where A is the diode contact area, A^* is the Richardson constant (32 Å·cm^{-2}·K^{-2} for p-type Si)[21] and Φ_{B0} is the zero-bias barrier height. Once I_0 is determined, Φ_{B0} is obtained by rewriting Eq. (2) as

$$\Phi_{B0} = \frac{kT}{q}\ln\left[\frac{AA^*T^2}{I_0}\right]. \quad (3)$$

The ideality factor, n, is introduced to take the deviation of the experimental *I–V* data from the ideal TE into account and it can be calculated from the slope of the linear region of the forward bias ln(*I*)–*V* plot and can be written as

$$n = \frac{q}{kT}\left(\frac{dV}{d(\ln I)}\right), \quad (4)$$

where $dV/d\ln(I)$ is the slope of the linear region of $\ln(I)$ versus V plots. Figure 2 shows the forward and reverse bias I–V characteristics of the fabricated photodiode under dark and various illuminations. The forward current in a wide voltage range (~ 0.2 V$< V <$ 1.5 V) exhibits a linear behavior and after 1.5 V, the $\ln I$–V plots are deviated from the linearity due to the effect of series resistance (R_s). The ideality factor (n) is obtained from the slope of the linear region of the forward bias $\ln I$–V plot. The barrier height (Φ_{B0}) of the device is calculated using Eq. (3). The n and Φ_{B0} values of the photodiode are found to be about 7.00 and 0.76 eV, respectively. The higher value of n, compared to the ideal value of 1, indicates that the photodiode exhibits a non-linear behavior.

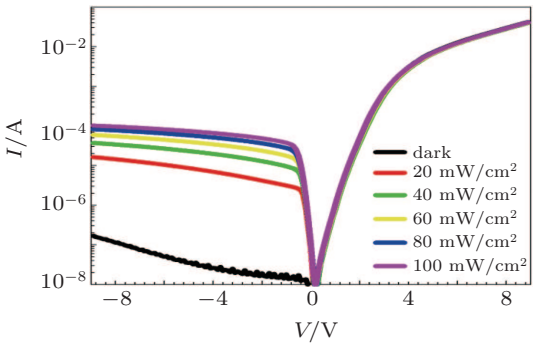


Fig. 2. (color online) Forward and reverse bias semi-logarithmic I–V characteristics of the photodiode under dark and different illuminations.

The high value of the n is attributed to the particular distribution of the interface states, the presence of inhomogenities of the barrier height, the thin film layer grown on the semiconductor wafer, series resistance, generation-recombination currents within the space-charge region, and tunneling might be other possible mechanisms that could lead to an ideality factor value greater than unity.[20,21,26–28]

As seen in Fig. 2, the forward currents of the diode under different illuminations did not change with illumination. The reverse current under a certain illumination is higher than that of the current under dark, and the reverse current of the diode increases with illumination intensity increasing. This is a strong clue that the fabricated diode exhibits a photodiode behavior. In order to analyze the photoconducting mechanism of the diode, we plot the photocurrent as a function of the light intensity in Fig. 3. The photoconducting mechanism of the diode is analyzed by the following relation[27,29,30]

$$I_{PH} = AP^m, \tag{5}$$

where I_{PH} is the photocurrent, A is a constant, m is an exponent, and P is the light intensity. The value of m is obtained from the slope of the $\log(I_{PH})$ versus $\log(P)$ plot and is found to be 0.88. The obtained m value in the range of 0.5 to 1 implies the presence of continuous distribution of trap levels.[29,30]

In order to analyze the contribution of high electric fields to current–voltage characteristics of the diode, I–V characteristics are plotted in double logarithmic scales in Fig. 4. As seen in Fig. 4, the $\ln(I)$–$\ln(V)$ plot has three distinct linear regions with different slopes (region 1: $-0.69 < V < 0.26$ V; region 2: $0.34 < V < 1.39$ V and region 3: $1.41 < V < 2.20$ V) that obey I–V^m change. Here, m is the slope of each region and was found to be 4.29, 6.30, and 3.01 for the photodiode in the dark. At the low bias region (region 1), the current approximately obeys a power law $I \sim V^{4.29}$, where the trap-charge limited conduction is dominant.[19,31–35] In the second region, the slope of the $\ln(I)$–$\ln(V)$ plot is larger than two and such behavior can be explained as a trap-charge limited current (TCLC) mechanism with an exponent trap distribution. At the higher bias region (region 3), because of the strong electron injection, the electrons escape from the traps and contribute to the space-charge-limited current (SCLC).[31–34]

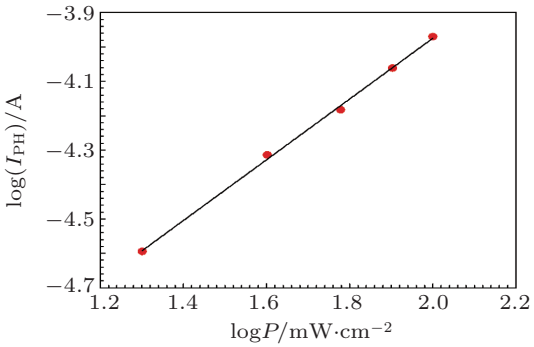


Fig. 3. (color online) Plot of $\log(I_{PH})$ versus $\log(P)$ of the photodiode (at bias voltage of −9 V).

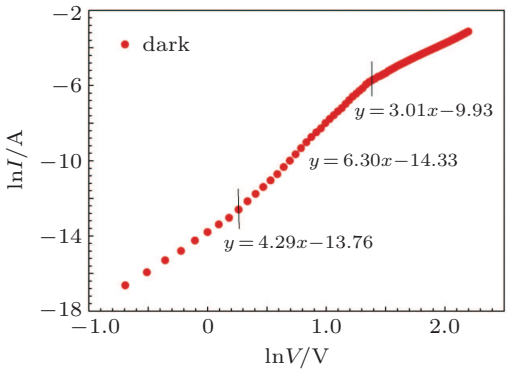


Fig. 4. (color online) Plot of $\ln(I)$ versus $\ln(V)$ of the diode.

The forward bias $\ln I$–V curve deviates from the linearity due to the effect of series resistance (R_s). The value of R_s is calculated using Cheung's method.[36] Cheung's functions are expressed by the following relations:

$$\frac{dV}{d(\ln I)} = IR_s + n\left(\frac{kT}{q}\right), \tag{6}$$

$$H(I) = V - n\left(\frac{kT}{q}\right)\ln\left(\frac{I}{AA^*T^2}\right) = n\Phi_{Bo} + IR_s. \tag{7}$$

Equations (6) and (7) give a straight line for the data in the downward curvature region of the forward bias I–V characteristics. In Figs. 5(a) and 5(b), experimental $\mathrm{d}V/\mathrm{d}\ln(I)$ versus I and $H(I)$ versus I plots are presented in the dark and 100 mW/cm^2 illumination intensity for the photodiode, respectively.

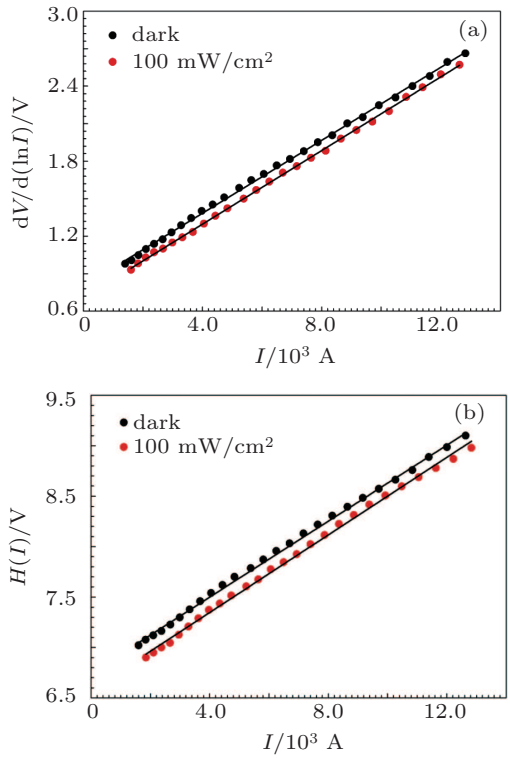


Fig. 5. (color online) (a) Experimental $\mathrm{d}V/\mathrm{d}\ln(I)$ versus I and (b) $H(I)$ versus I plots of the photodiode in the dark and 100 mW/cm^2 illumination intensity.

The values of R_s are obtained from the slopes of the $\mathrm{d}V/\mathrm{d}\ln(I)$ versus I and $H(I)$ versus I plots. The calculated values of R_s from Figs. 5(a) and 5(b) in the dark and 100 mW/cm^2 are found to be 147.18 Ω and 145.83 Ω, and 187.98 Ω and 183.54 Ω, respectively. As a result, the obtained R_s values using Cheung's functions are in good agreement with each other.[15,29,37–41]

Furthermore, it is well known that the parasitic resistances such as series resistance (R_s) and shunt resistance (R_sh) affect the current–voltage characteristics of the device. Thus, it is important to determine these parameters to explain the performance of the photodiode. The resistance of the photodiode can be expressed as

$$R_\mathrm{i} = \frac{\mathrm{d}V_\mathrm{i}}{\mathrm{d}I_\mathrm{i}}. \tag{8}$$

The voltage dependent resistance profile of the photodiode in the dark and under various illumination intensities at room temperature was obtained from the I–V data using Eq. (8) and is given in Fig. 6. As seen in Fig. 6, at sufficiently high forward bias region (about 9 V), the value of resistance corresponds to the R_s for the photodiode.

On the other hand, the value of resistance in the negative bias region (about −9 V) corresponds to the R_sh of the photodiode. The values of R_s and R_sh for the photodiode in the dark and under different illumination intensities are found to be ∼ 174 Ω and 53 MΩ, and ∼ 162 Ω and 88 kΩ, respectively. It is observed that the values of R_s and R_sh are decreased with illumination intensity increasing. As a result, it is well known that the ideal devices require the lower series resistance and a higher shunt resistance. Similar results are found in Refs. [42] and [45].

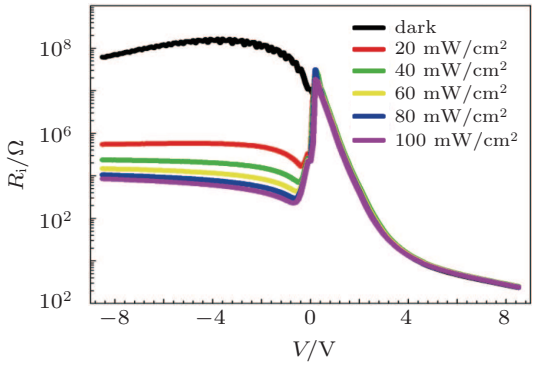


Fig. 6. (color online) Plots of R_i versus V of the photodiode in the dark and under various illumination intensities.

4. Conclusions

In conclusion, a novel spinel ferrite (Al/AlFe$_2$O$_4$/p-Si) Schottky photodiode was successfully fabricated via the sol–gel coating process. The analysis of the reverse and forward bias I–V characteristics of the fabricated photodiode have been investigated under different illumination conditions. The main electrical parameters such as n, Φ_B0, and R_s values were obtained from the forward and reverse bias I–V characteristics. The obtained results show that the photodiode exhibits a high photosensitivity. We believe that the fabricated spinel ferrites for the Schottky photodiode will open a new avenue of spinel structure and related materials for optoelectronic device applications in the near future.

References

[1] Adurodija F O, Semple L and Bruning R 2005 *Thin Solid Films* **492** 153
[2] Chen H Y and Wu J H 2012 *Appl. Surf. Sci.* **258** 4844
[3] Minami T 2005 *Semicond. Sci. Technol.* **20** S35
[4] Bhosale C H, Kambale A V, Kokate A V and Rajpure K Y 2005 *Mater. Sci. Eng. B* **122** 67
[5] Champness C H and Xu Z 1998 *Appl. Surf. Sci.* **123–124** 485
[6] Stadler A 2012 *Materials* **5** 661
[7] Cruz J S, Delgado G T, Perez R C, Romero C I Z and Angel O Z 2007 *Thin Solid Films* **515** 5381
[8] Bian J M, Li X M, Gao X D, Yu W D and Chen L D 2004 *Appl. Phys. Lett.* **84** 541
[9] Subramanyam T K, Uthanna S and Naidu B S 1998 *Mater. Lett.* **35** 214
[10] Gupta R K, Cavas M and Yakuphanoğlu F 2012 *Spectrochimica Acta Part A* **95** 107
[11] Lind C, Gates S D, Pedoussaut N M and Baiz T I 2010 *Materials* **3** 2567

[12] Ellmer K 2001 *J. Phys. D: Appl. Phys.* **34** 3097
[13] Sileo E E, Rodenas L G, Paiva-Santos C O, Stephens P W, Morando P J and Blesa M A 2006 *J. Solid State Chem.* **179** 2237
[14] Valenzuela R 1994 *Magnetic Ceramics* (Cambridge: Cambridge University Press)
[15] Soylu M, Al-Ghamdi A A and Yakuphanoğlu F 2012 *Microelectronic Eng.* **99** 50
[16] Akkal B, Benemara Z, Bachir Bouiadjra N, Tizi S and Gruzza B 2006 *Appl. Surf. Sci.* **253** 1065
[17] Osvald J 2006 *Solid State Electron.* **50** 228
[18] Pür F Z and Tataroğlu A 2012 *Phys. Scr.* **86** 035802
[19] Demirezen S, Altındal Ş and Uslu İ 2013 *Current Appl. Phys.* **13** 53
[20] Rhoderick E H and Williams R H 1988 *Metal-Semiconductor Contacts* (2nd edn.) (Oxford: Clarendon Press)
[21] Sze S M 1981 *Physics of Semiconductor Devices* (2nd edn.) (New York: John Wiley & Sons)
[22] Wang S G, Zhang Y, Zhang Y M and Zhang Y M 2010 *Chin. Phys. B* **19** 017203
[23] Chand S and Bala S 2005 *Semicond. Sci. Technol.* **20** 1143
[24] Tataroğlu A 2013 *Chin. Phys. B* **22** 068402
[25] Chand S 2004 *Semicond. Sci. Technol.* **19** 82
[26] Mamor M 2009 *J. Phys. Condens. Matter* **21** 335802
[27] Gupta R K, Al-Ghamdi A A, Al-Hartomi O, Hasar H, El-Tantawy F and Yakuphanoğlu F 2012 *Synth. Met.* **162** 981
[28] Reddy V R, Reddy M S P, Lakshmi B P and Kumar AA 2011 *J. Alloys Compd.* **509** 8001
[29] Yakuphanoğlu F and Senkal B F 2009 *Synthetic Metals* **159** 311
[30] Kazım S, Alia V, Zulfequar M, Haq M M and Husain M 2007 *Physica B* **393** 310
[31] Uslu H, Altındal Ş, Polat İ, Bayrak and Bacaksiz E 2010 *J. Alloys Compd.* **509** 5555
[32] Farag A A M, Ashery A, Ahmed E M A and Salem M A 2010 *J. Alloys Compd.* **495** 116
[33] Ocak Y S, Kulakçı M, Kılıçoğlu T, Turan R and Akkiliç K 2009 *Synth. Met.* **159** 1603
[34] Taşçıoğlu İ, Aydemir U and Altındal Ş 2010 *J. Appl. Phys.* **108** 064506
[35] Phan D T, Gupta R K, Chung G S, Al-Ghamdi A A, Al-Hartomy O, El-Tantawy F and Yakuphanoğlu F 2012 *Solar Energy* **86** 2961
[36] Cheung S K and Cheung N W 1986 *Appl. Phys. Lett.* **49** 85
[37] Gupta R K and Yakuphanoğlu F 2012 *Solar Energy* **86** 1539
[38] Aldemir D A, Esen M, Kökçe A, Karataş Ş and Özdemir A F 2011 *Thin Solid Films* **519** 6004
[39] Tataroğlu A, Altındal S and Bülbül M M 2006 *Nucl. Instr. and Meth. A* **568** 863
[40] Sochacki M, Kolendo A, Szmidt J and Werbowy A 2005 *Solid State Electron.* **49** 585
[41] Karataş Ş and Altındal Ş 2005 *Mater. Sci. Eng. B* **122** 133
[42] Donoval D, Barus M and Zdimal M 1991 *Solid State Electron.* **34** 1365
[43] Karimov K S, Ahmed M M, Moiz S A and Federov M I 2005 *Sol. Energy Mater. Sol. Cells* **87** 61
[44] Mansoura Sh A and Yakuphanoğlu F 2012 *Solid State Sci.* **14** 121
[45] Janardham V, Lee H K, Shim K H, Hong H B, Lee S H, Ahn K S and Choi C J 2010 *J. Alloys Compd.* **504** 146